Paper Title: Estimating Reservoir Sedimentation Using Deep Learning

Authors: Amanda L. Cox; Deanna Meyer; Alejandra Botero-Acosta; Vasit Sagan; Ibrahim Demir; Marian Muste; Paul Boyd; and Chandra Pathak

Affiliations: WATER Institute (Cox, amanda.cox@slu.edu; Meyer, deanna.meyer@slu.edu; Botero Acosta, alejandra.boteroacosta@slu.edu) and Taylor Geospatial Institute (Sagan, vasit.sagan@slu.edu), Saint Louis University, St. Louis, Missouri, USA; Civil and Environmental Engineering (Demir, ibrahim-demir@uiowa.edu) and IIHR- Hydroscience & Engineering (Muste, marian-muste@uiowa.edu), University of Iowa, Iowa City, Iowa, USA; US Army Corps of Engineers (Boyd, Paul.M.Boyd@usace.army.mil; Pathak, Chandra.S.Pathak@usace.army.mil), Omaha, NE and Washington, DC, USA. (Correspondence to Cox: amanda.cox@slu.edu).

This paper is a non-peer reviewed preprint submitted to Earth ArXiv.

This paper has been submitted to the ASCE Journal of Hydrologic Engineering for publication consideration.

Estimating Reservoir Sedimentation Using Deep Learning

Amanda L. Cox, M.ASCE[1]; Deanna Meyer[1]; Alejandra Botero-Acosta[1]; Vasit Sagan[2]; Ibrahim Demir[3]; Marian Muste[3]; Paul Boyd[4]; and Chandra Pathak[4]

Abstract: Several reservoirs across the US are filling with sediment, which jeopardizes their functionality and increases maintenance costs. The US Army Corps of Engineers (USACE) developed the Reservoir Sedimentation Information (RSI) system to assess reservoir aggradation and track dam operation suitability for water-resource management and dam safety. The RSI dataset contains historical elevation-capacity data for approximately 400 dams (excluding navigation structures) which correspond to less than 1% of dams across the US. Thus, there is a critical need to develop methods for estimating reservoir sedimentation for unmonitored sites. The goal of this project was to create a generalized method for estimating reservoir sedimentation rates using reservoir design information and watershed data. To meet this objective, geospatial tools were used to build a refined composite dataset to complement the RSI system's data with precipitation and watershed characteristics. Nine deep learning models were then used on the benchmark dataset to determine its accuracy at predicting capacity loss for the RSI reservoirs: four supervised machine learning models, four deep neural network (DNN) models, and a multilinear power regression model. A DNN model, containing a progressively increasing node and layer construction, was deemed the most accurate, with R^2 values from its calibration and validation datasets being 0.83 and 0.70, respectively. The best model was recalibrated over the entire dataset, which showed greater accuracy on the prediction of RSI reservoir's capacity loss, with an R^2 of 0.81. This predictive model could be used to evaluate the capacity loss of unmonitored reservoirs, forecast sedimentation rates under future climate conditions, and identify reservoirs with the highest risk of losing functionality.

Keywords: Reservoir Sedimentation; Reservoir Capacity; Machine Learning.

1. Introduction

Dams and their associated reservoirs enable water storage, flood control, hydroelectric power generation, and supply reliable water resources for various socio-economic needs. However, reservoirs throughout the nation are slowly filling with sediment, diminishing their life cycle and reducing their effectiveness, while increasing their cost of maintenance (Sholtes et al., 2018). The immediate consequences of sediment retention in reservoirs are diminishing reservoir capacity, creation of backwater flooding upstream, as well as impairing turbines of the structure (Morris and Fan, 1998). The costs of remediating accumulated sediment in these structures may be exceedingly expensive, with dam removal providing the greatest expense in dam decommissioning options (U.S. Bureau of Reclamation, 2006).

Existing reservoir sedimentation models have been unable to analyze the intricate large-scale temporal or spatial patterns of sedimentation due to a lack of available data required for model calibration and validation. The typical data required for model construction include daily to yearly hydrologic records, bathymetric reservoir details, and grain-size distribution of sediment (Ackers, 1988; Lajczak, 1996; Tarela and Menendez, 1999; Sundborg, 1992; Rowan et al., 2001). The most valuable support for reservoir sedimentation model development in recent times has been provided by Geographic Information System (GIS) tools that enables the addition of land use over large scales to the hydrologic data (Verstraeten et al., 2003; Vorosmarty et al., 2003, Lehner et al., 2011). However, GIS tools are relatively new hence their historical records are too short to refine sedimentation modeling (Xu et al. 2019). This lack of temporal data in sedimentation modeling

60 diminishes the ability for proper model calibration, which has shown in sediment yield estimated
61 values to deviate considerably from measured sediment yield rates (Trimble, 1999).

62 The U.S. Army Corps of Engineers (USACE) oversees several dams and reservoirs across the
63 US, with many of them being under operation for more than 50 years (Pinson et al., 2016). The
64 aging of these USACE reservoirs makes them at greater risk for complications related to
65 sedimentation. Reservoir capacity surveys focused on US reservoir sedimentation trends indicate
66 that they could deplete by as much as 10%-35% of absolute water storage capacity (Randle et al.,
67 2019). These historical surveys are invaluable tools for identifying past and present regional
68 sedimentation trends, allowing for the evaluation of sediment aggradation and life expectancy of
69 individual reservoirs. These data are also relevant for developing effective reservoir management
70 strategies. Ensuing from the above, the USACE initiated the Enhancing Reservoir Sedimentation
71 Information for Climate Preparedness and Resilience (RSI) program to assess reservoir
72 aggradation and track dam operation suitability for water-resource management. However, since
73 the RSI dataset contains less than 1% of the US dams, developing methods for estimating reservoir
74 sedimentation at unmonitored sites is needed.

75 Machine learning as a tool for prediction and anomaly detection has developed rapidly over
76 the last couple of decades. Through several research studies, machine learning has been proven to
77 be successful at predicting streamflow, sediment transport, sediment deposition, and water-quality
78 characteristics as well as identifying data anomalies (Xiang and Demir, 2020; Azamathulla et al.,
79 2010; Choubin et al., 2017; Peterson et al., 2019; Xu et al., 2019; Peterson et al., 2020; Bhadra et
80 al., 2020; Hazarika et al., 2020). Due to the nonlinear behavior of sedimentation processes
81 influenced by various hydraulic flow factors, the use of machine learning has great potential for

constructing accurate reservoir capacity loss at unmonitored sites compared to alternative methods (Adnan et al., 2019; Baniya et al., 2019). Machine learning utilizes the process of iteration and probabilistic pattern detection to determine the relationship between input parameters and a dependent variable (Geron, 2022). Prior to utilization of machine learning applications, the sediment yield and sediment load, as well as estimated water pollutants was obtained through various process-based modeling (Ayele et al., 2017; Zounemat-Kermani et al., 2019; Zounemat-Kermani et al., 2020).

Machine learning modeling applied to reservoir sedimentation is not, however, infallible as shown by the backpropagation networks used to assess sediment transfer occurring under differing land use and agricultural practices (Abrahart and White, 2001). The valuable insights provided by an artificial neural network model trained on 32 years of reservoir sedimentation data for one reservoir (Jothiprakash and Garg, 2009) indicates that the availability of long-term data is critical for trustful modeling outcome. It is however obvious that training machine learning requires not only long-term data but also a great variety of reservoir in order to be more reliable and generalizable.

The RSI system provides a good baseline resource for training data-driven models that could be utilized for improved reservoir sedimentation estimation modeling through its combination of temporal and spatial data spanning the contiguous US. The objective of this research was to create a generalized deep learning method for estimating reservoir sedimentation using reservoir design data and supplemental watershed information. To achieve this objective, the following tasks were completed: 1) the RSI dataset was analyzed to determine capacity loss between consecutive surveys, 2) supplemental hydrologic data were derived for each reservoir and set of consecutive

surveys (e.g., basin area and cumulative precipitation), 3) multiple deep learning algorithms were applied using the composite dataset to create models to predict reservoir sedimentation, and 4) model performances were analyzed and compared to identify a recommended model for industry use. This prediction tool will allow the estimation of current conditions of unmonitored reservoirs and forecast future sedimentation rates for reservoirs within the US.

2. Composite RSI Dataset Development

RSI information for 184 reservoirs was combined with supplementary watershed information related to hydrologic and sedimentation processes to form the composite RSI dataset utilized in this study. Each record of this dataset corresponded to two consecutive surveys conducted by the USACE at that particular reservoir, and the capacity loss for each record was the difference in the reservoir's capacity at the maximum pool elevation that was not characterized as a surcharge pool.

The RSI composite dataset incorporated data remotely compiled through publicly available sources to ensure comprehensive watershed characteristics were associated with each recorded reservoir's capacity loss. Utilization of raster datasets enabled the extraction of relevant hydrologic data, which were identified and applied to their respective basins within the composite database. These public databases provided data related to climatologic, topographic, and erosion processes occurring across the associated watersheds, for each record within the composite dataset. Fig. 1 shows the features collected per each reservoir record, including the originally provided USACE RSI system data, and the accessed public database. Reservoir features and basin characteristics within the dataset were assumed constant over time for each reservoir. Thirty-two variables compose the composite RSI dataset, including numerical variables (27), identifier variables (2),

categorical variables (2), and a date variable. Missing data records were replaced with the mean for that specific variable.

The watershed centroid latitude and longitude values for each reservoir were extracted from each basin's shapefile. The curve number (CN) and the erodibility values were computed for each reservoir as the area-weighted average for its associated basin. The CN is the empirical hydrologic parameter indicative of a catchment's runoff potential based on soil and land use characteristics (USDA, 1986), while the erodibility index is an empirical measure of the inherent resistance of geologic materials (soils and rocks) to erosion. The CN maps were based on national soil and national land cover (NLCD) raster files (Viger and Bock, 2014; USGS, 2017). Utilizing USGS characteristics for soil hydrologic groupings, and land use categorization, the CN values were defined based on guidelines found in the Revised Universal Soil Loss Equation (RUSLE) for each soil type (Renard, 1997). The average erodibility indices for sand (0.125), loam (0.325), and clay (0.1) were used to create erodibility maps for each reservoir's basin based on the national soils map (Viger and Bock, 2014). Additionally, the NLCD was used to compute the percent of forested area within a reservoir's basin, with deciduous, evergreen, and mixed forest types consolidated into one category for this study.

Google's Earth Engine facilitated the extraction and computation of variables from U.S. Digital Elevation Models (DEMs) and monthly precipitation maps (US Geological Survey, 2017; Gorelick et al., 2017). For this analysis, a 1/3rd arc-second DEM was utilized for calculating features reliant on topographic information for the 184 reservoir basins within the composite dataset. These features include hydraulic length, basin elevation, average slope, area, and relief, which was defined as the difference between the maximum and minimum elevation. Based on

147 these calculations, the channel slope was estimated as the relationship of the relief divided by the
148 hydraulic length. A reservoir's initial trap efficiency (E) was calculated as a reservoir's initial
149 capacity in m^3 (C), and a reservoir's drainage area in km^2 (A) shown in Eq. (1) (Brown, 1943).

150 $$E = 1 - \frac{1}{1+(2.1\times10^{-4})C/A} \quad \text{(Eq. 1)}$$

151 Further, precipitation data for each reservoir was found by analyzing 30 arc-second monthly
152 precipitation raster files (Daly *et al.*, 2015) that aligned with the database's time periods per each
153 set of consecutive surveys. Additionally, cumulative, maximum, mean, and median monthly
154 precipitations for each record were calculated. Further, the computation of normalized maximum
155 precipitation equaled the maximum precipitation divided by the mean monthly precipitation.

156 Since many dams were built upstream of RSI reservoirs, a batch analysis was employed to
157 include upstream dam heights, as well as the maximum, and normal storage of each reservoir
158 within the RSI composite dataset. This computation was conducted in two steps: 1) Utilize the
159 National Inventory of Dams (NID) dataset, composed of over 90,000 U.S. dams, to create an
160 annual time series of cumulative upstream dam height, and normal and maximum storage for each
161 RSI reservoir; 2) time average the upstream dam's variables, for the period of time comprising two
162 subsequent surveys for each RSI dataset record.

163 ***2.1. Dataset Pre-Processing***

164 Due to natural processes, sustained or increases in reservoir capacity are not possible, unless
165 dredging or free-flow sediment flushing has been employed (Wang and Hu, 2009). Thus, a
166 reservoir's capacity will decrease over time. With this knowledge, the RSI composite dataset
167 records containing identical capacities, or an increased trend in capacity between a set of

consecutive surveys, were removed. Additionally, sets of consecutive surveys containing identical survey data or dates were filtered out.

A log transformation (Brakstad, 1992; Emmerson *et al.*, 1997), was applied to the numerical variables of the RSI composite dataset to remove the impact of the difference in orders of magnitude. The following provides the equation for the log transformation:

$$x_{l_i} = \text{sgn}[\ln(|x_i| + 1)] \quad \text{Eq. (2)}$$

where x_i is the original data value; x_{l_i} is the log-transformed value; i is the number of observations; and the sgn function multiplies the value by either a value of one if x_i is a positive value or a value of negative one if x_i is a negative value. Additionally, a minimum-maximum (min-max) normalization (Goyal *et al.*, 2014; Patro and Sahu, 2015) of the numerical variables was conducted using the following equation:

$$x_{lm_i} = 0.7\left(\frac{x_{l_i} - x_{l\_min}}{x_{l\_max} - x_{l\_min}}\right) + 0.15 \quad \text{Eq. (3)}$$

where x_{lm_i} is the log-transformed and min-max normalized value; x_i is the original data value; x_{l_i} is the log-transformed value; where x_{l_min} is the minimum value of the x_l dataset; x_{l_max} is the maximum value of the x_l dataset. This results in a linear scaling with values ranging from 0.15 to 0.85. The min-max normalization of data fits the data in a pre-defined range keeping the relationships from the original data unchanged (Patro and Sahu, 2015).

Depending on the performance of models, standard scaling was applied in lieu of the min-max normalization. This normalization method minimizes the number of parameters that appear constant across the dataset, which can affect model performance. Standard scaling centers the dataset values around the mean with a unit of standard deviation (Cao *et al.*, 2016). The following equation details the standard scaling calculations:

$$x_{ls_i} = \frac{x_{l_i} - \mu}{\sigma} \quad \text{Eq. (4)}$$

where x_{ls_i} is the log-transformed scaled value; μ is the mean of the x_{l_i} dataset; and σ is the standard deviation of the x_{l_i} dataset.

3. Methods

The dataset compiled for the RSI reservoir sites consisted of variables relevant to sedimentation and hydrologic processes. Transformation and scaling of the dataset were performed to diminish bias and skew of the variables' distribution. A feature importance analysis was conducted to analyze the sensitivity of variables detrimental to model performance, which resulted in the creation of a dataset with decreased variable size. The original and the feature-importance-derived datasets were used to develop and evaluate capacity loss prediction models. Both sets of data were examined in each iteration of the statistical or machine learning method. For all models analyzed, a 70/30 split of the dataset was applied for the training and testing of the models, respectively.

The first statistical model used was the Ordinary Least Squares (OLS) multilinear regression model. The second analysis consisted of four supervised machine learning regression models: Support Vector Machine (SVM), Random Forest (RFR), Decision Tree (DTR), and Partial Least Squares (PLS). The third analysis used deep neural network (DNN) models. In the DNN model survey, four base DNN architectures were analyzed.

A data anomaly detection was performed to reduce erroneous data within the composite dataset. This included anomaly removals utilizing Autonomous Anomaly Detection (AAD) (Angelov et al., 2016; Gu and Angelov, 2017), which flagged 18 records corresponding to 15 reservoirs, and the Kolmogorov-Smirnov and Efron (KSE) outlier detection method (Jirachan and

Priomsopa, 2015), which flagged 15 records corresponding to 10 reservoirs. Removal of anomalous data from data used in model development varied by model based on performance.

Lastly, seven metrics were used to compare all created models. The following performance parameters were quantified for evaluation and goodness-of-fit analysis of the statistical models: coefficient of determination (R^2), Mean Absolute Percent Error (MAPE), Root Mean Square Error (RMSE), and Relative Root Mean Square Error (RRMSE). The remaining three parameters included the Percent Bias (PBias), the ratio of root mean squared error to standard deviation of measured data (RSR), and the Pearson Correlation Coefficient (r), to help analyze the models' overall accuracy outside the limitations of correlation-based measures (Legates & McCabe, 1999). Respectively, these three metrics were used to quantify each model's overestimation or underestimation, normalization to error index evaluation in model performance (Moraisi et al., 2007), and uncover the degree of linear association between calibrated and observed values of the model (Taylor, 1990; Adler and Parmyryd, 2010). Collectively, watershed model performance metrics can be considered satisfactory if $R^2 > 0.5$, PBias + 55%, RSR < 0.7, and r > 0.5 (Moriasi et al., 2007; Ayele et al., 2017).

3.1. Feature Correlation and Recursive Feature Elimination (RFE)

A Spearman's rank correlation calculation was performed to measure the monotonic relationship across predictor variables. Ranging from -1 to 1, the Spearman's calculated coefficient gauges whether two features are correlated, with -1 being negatively correlated and 1 being positively correlated (Bon-Gang, 2018). Determining these relationships between the predictor variables was necessary to investigate potential collinearity shared across the composite dataset, and if removal

of features could improve ensuing model performance. The general criterion for modeling a regression analysis is a minimum of 10 to 20 samples per predictor variable (Austin and Steyerberg, 2015).

To observe if reducing the number of predictor variables in the composite dataset improved results, a *Recursive Feature Elimination* (RFE) algorithm was performed from which an alternative dataset was developed. Utilizing optimized random forest model parameters, the RFE was used to establish the optimal amount of predictor variables for this new RFE-determined dataset. The RFE algorithm assigns weights to features based on model performance. The significance of this algorithm is its allowance to choose the number of features desired in the reduced dataset, and its theoretical improvement within statistical modeling through its removal of collinear features. The presence of numerous collinear features can lead to overfitting when analyzing the prediction of dependent variables through machine learning models (Harrell, 2001).

3.2. Ordinary Least Squares Multilinear Regression

The Ordinary Least Squares (OLS) multilinear regression model is used for relational analysis between one or more variables. The method corresponds to the minimization of the sum of the square error difference between the observed and predicted values of the target variable, as it fits an assumed linear relationship between the explanatory variables (Zdaniuk, 2014). The OLS regression formula to compute capacity loss, y_i:

$$y_i = \beta_0 + \beta_1 x_{l_{i1}} + \beta_2 x_{l_{i2}} + \cdots + \beta_p x_{l_{ip}} + \epsilon \qquad \text{Eq. (6)}$$

where i is the number of observations, y_i is the dependent variable, x_{l_i} are the explanatory variables, β_0 is the y-intercept or constant term of the equation, β_p is the slope coefficients for each explanatory variable, and ϵ is the residuals of the model (Alexopoulos, 2010). Standard

scaling was used to evaluate the magnitude of influence each predictor variable had on the target variable. Imperial system units were used for the OLS analysis and due to regression model complexity, all International System of Units (SI) values must be converted to imperial units for application. When using the OLS method with metric units, the SI value of each input parameter should be multiplied by the corresponding metric unit conversion factor listed in Table 1 prior to the log-transformation in Eq. 2. Similarly, the capacity loss term, y_i, computed from Eq. 6 is in acre-ft and needs to be multiple by 1,233 for conversion to m^3.

3.3. Supervised Machine Learning

Supervised machine learning is the application of algorithms capable of producing generalities in patterns via the use of externally supplied data to predict future patterns and instances (Singh *et al.*, 2016). Several types of supervised machine learning algorithms exist, but for this analysis SVM (Noble, 2006), RFR (Breiman, 2001), DTR (Bashar *et al.*, 2019), and PLS (Manikanta et al., 2015) regression algorithms were utilized. Each algorithm has advantages and disadvantages when applied to a unique dataset; thus, implementation of these four enabled comprehensive analysis of supervised learners on the composite and RFE datasets. Additionally, each supervised learner used a pipeline of several intermediary steps, that chained a sequence of estimators for optimization and cross-validation of model performance. These steps included a principal component analysis and standard scaling. These optimizing components were refined by automated selection of each model's hyperparameters resulting in the highest performing variation of the supervised model.

3.4. Deep Neural Network (DNN)

A DNN is an organized collection of neurons sequenced into multiple layers for determining modeled predictions. The neurons receive input from the initial dataset if they reside within the

first layer of the DNN, or from input from activated neurons from previous layers if residing within a subsequent layer. The activations of the neurons occur based on a calculation of the weighted sums from that input followed by a nonlinear activation (Montavon *et al.*, 2018). In the case of this analysis, the Rectified Linear (ReL) activation function was used. All nodes that consist of this activation function are considered rectified linear activation units (ReLU), whose development was a milestone in the evolution of deep learning (Goodfellow *et al*., 2016). Deep learning (DL) studies have gained significant momentum with the availability of computational resources, benchmark datasets (Demir et al., 2022; Sit et al., 2021a), and the popularity of DL algorithms in many data analysis tasks in water resources and hydrology including streamflow forecasting (Sit et al., 2022b), culvert sedimentation (Xu *et al.*, 2019), data augmentation (Demiray *et al.*, 2021), and image synthesis (Gautam *et al.*, 2022).

For this analysis, four DNN architectures were utilized, and the models were optimized to minimize the mean absolute error (MAE). The basis of the first DNN architecture was used in the research of Maimaitijiang *et al*. (2020), which contained a GIS and remotely sensed dataset. Named DNN-F1, it incorporated a DNN node structure that continually increased in complexity per each layer. The minimum number of nodes residing within the initial layer was 64, and the maximum number of nodes retained within the final layering was 1024. For the purposes of this study, this first progressively increasing DNN (termed DNN_{PI1}), will be the base DNN used to compare further DNN architectures. The second DNN architecture was aimed at analyzing if information bottlenecking could improve the initial DNN. The bottlenecking method aims to balance improved accuracy through decreasing complexity (Tishby *et al*., 2000; Hecht and Tishby, 2005). This version of the DNN reverses the initial architecture to become a progressively

decreasing DNN (termed DNN_{PD1}), which results in its initial layer containing a node network of 1024, and its final layer containing a node network of 64. Schematics of the DNN_{PI1} and DNN_{PD1} architectures are shown in Fig. 2.

Two simplified DNN structures were also evaluated to determine their performance compared to the complex DNN_{PI1} and DNN_{PD1} structures: a second progressively increasing DNN (termed DNN_{PI2}) and a second progressively decreasing DNN (termed DNN_{PD2}). Detailed node architectures for these simpler DNNs are shown in Fig. 3. The DNN_{PI2} and DNN_{PD2} structures have half the number of layers as the DNN_{PI1} and DNN_{PD1}, and fewer nodes associated with each of their layers. The DNN_{PI2} structure contains an initial neural structure that starts with 8 nodes and increases to 32 in its final layer. The DNN_{PD2} structure is the reversed iteration of the DNN_{PI2}.

4. Results and Discussion

4.1. Feature Importance Analysis

To identify collinearity or monotonic relationships between features, a Spearman's rank coefficient matrix analysis was performed. Values closest to 1 or -1 were respectively deemed highly positively or negatively correlated. The digital elevation model (DEM) parameters showed a significant positive correlation with each other, as well as basin relief with values ranging from 0.57 to 0.92. Alternatively, the DEM parameters appear negatively correlated to the monthly precipitation parameters with values of -0.54 to -0.66. This analysis signifies that the compiled features within the dataset contain redundancies.

4.2. Recursive Feature Elimination (RFE)

The Recursive Feature Elimination (RFE) algorithm was applied to reduce potentially redundant features and further optimize the performance of the predictive models. The composite dataset

consisted of 467 samples with 27 predictor variables. Thus, the dataset had a ratio of approximately 17 samples per predictor variable within the dataset. When reducing composite dataset features, the RFE conducts its model accuracy performance based on R^2 values, with 1.00 being the highest accuracy score possible. The RFE results showed that twelve predictor variables retained an R^2 value of between 0.78 – 0.80. With less than twelve variables, the accuracy scored less than or equal to 0.77. Thus, the twelve predictor variables listed in Table 1 were optimal in minimizing the composite dataset to a sample-to-feature ratio of approximately 38. This new RFE dataset was used in subsequent models and the results were compared to the entire composite dataset. Standard scaling was used to help further analyze the magnitude of influence each predictor variable had on the target variable, within the OLS equation.

The inclusion of basin relief, hydraulic length, and the channel slope features within the RFE dataset, may be seen as still maintaining excessive collinear features. However, due to the logarithmic transformation and normalizations performed on the data, the feature of channel slope, which is derived from hydraulic length and basin relief, is mathematically unique in terms of providing a predictive value within the model's equation.

Three features are indicators of drainage basin size: basin area, hydraulic length, and basin relief. The basin area model coefficient of 0.548 indicates that area is the dominant feature related to basin size. Based on the Spearman correlation analysis, both basin length and relief are positively correlated with capacity loss. However, both the length and relief coefficients are inversely related to the predictive variable (i.e., capacity loss) suggesting their model contribution is an adjustment on the basin area influence.

All models developed using the RFE dataset resulted in improved performance compared to models from the entire composite dataset. Due to the large number of models generated, only the RFE results are reported.

4.3. OLS Regression Model

The log-transformed RFE dataset with no anomalies removed was found to produce the best OLS model performance. The observed versus predicted training and testing results for the OLS model are shown in Fig. 4. Following the training/testing analysis, the OLS model was calibrated using the full dataset to provide the overall best-fit equation. Figure 4 also shows the observed versus predicted values for the calibrated OLS model which had an R^2 value of 0.40 and a MAPE of 195%. Equation (7) provides the OLS prediction equation based on the coefficient values and constant terms derived from the calibrated OLS model results:

$$y_{OLS_l} = -9.71 + 0.548x_{l_1}U_1 + 0.476x_{l_2}U_2 + 0.383x_{l_3}U_3$$
$$-0.169x_{l_4}U_4 + 0.561x_{l_5}U_5 + 1.59x_{l_6}U_6$$
$$-0.0460\,x_{l_7}U_7 + 0.0250x_{l_8}U_8 - 0.0249x_{l_9}U_9$$
$$+1.87x_{l_{10}}U_{10} + 0.188x_{l_{11}}U_{11} + 0.0588x_{l_{12}}U_{12} \qquad \text{Eq. (7)}$$

where y_{OLS_l} is the log-transformed predicted capacity; x_{l_p} are the log-transformed predictor variables; U_p is the metric unit conversion factor; and the numeric subscript p on the x_l and U terms denotes the variable index (Table 1). To obtain the predicted capacity loss value, the model predicted value (y_{OLS}) needs to be un-transformed using Eq.(8):

$$y_{OLS} = (e^{y_{OLS_l}} - 1\,) * 1233 \qquad \text{Eq. (8)}$$

4.4. Supervised Machine Learning

The best performing supervised machine learning model was identified based on the satisfactory statistical metrics defined by Moriasi et al., 2007. Nearly all the supervised machine learning models had optimal performance when using the log-transformed normalized RFE dataset with the KSE anomalies removed. The supervised machine learning results presented within this report were all developed using this dataset. A comparison between the supervised machine learning methods showed that the RFR had the most accuracy, in terms of predictive performance, when trained and tested on the respective data. With a training set R^2 of 0.61 and a testing set R^2 of 0.57, the model shows precision in model fitness when comparing the predicted versus observed values of capacity loss. Tables 2 and 3 show the performance metrics of the training and testing results for this model. Notably, there is a significant increase in MAPE on the testing dataset's forecasting accuracy. This signifies that the model training results are overestimating the model's performance, regardless of the relatively high R^2 value present on the testing dataset.

4.5. DNN Analysis

All the DNN models had optimal performance when using the log-transformed normalized RFE dataset with the KSE anomalies removed. The DNN results presented for this study were developed using this dataset. The complex DNNs had significantly better accuracy based on the MAPE and R^2 values. The DNN_{PI1} was identified as the best DNN model variation based on maximizing the R^2 and minimizing the RRMSE. Training and testing results for this DNN model are shown in Table 3. The DNN_{PI1} had training and testing R^2 values of 0.83 and 0.70, respectively. This makes the DNN_{PI1} the best fitting model in terms of performance. The RRMSE values of the DNN_{PI1} were the lowest RRMSE values compared across all analyzed machine learning models.

However, the MAPE and RRMSE values showed a relatively large percentage increase between training and testing, meaning there may be underlying forecasting inaccuracies.

4.6. Comparison of Models

A comparison of the supervised machine learning, DNN, and OLS models is shown in Fig. 4; model summary statistics for the untransformed model data are provided in Table 2 and Table 3**Table 3**. All models were developed using the transformed data, but the prediction variable of interest is the capacity loss (i.e., not the log-transformed capacity loss). Thus, untransformed statistics were used to assess model performance and their values are reported on all observed versus predicted plots. Further, results shown are for the RFE dataset (feature variables listed in Table 1) as the RFE dataset performed better than the original composite dataset for all models analyzed. Except for RFR, the supervised machine learning methods resulted in abnormal predictive performance. However, the RFR, and the more complex DNNs, showed promising results in terms of learning and predicting capacity loss. Overall, the best tested model performance, based on R^2 and RRMSE, was the DNN_{PI1} with an untransformed R^2 value of 0.70 and an untransformed RRMSE of 135%.

The RRMSE values measured across all models, as they relate to the OLS RRMSE value are shown in Fig. 5. The OLS method of prediction compared respectably when set side by side with more computationally complex machine learning models in terms of R^2 and MAPE. However, the more complex models did result in considerably lower RRMSE values, compared to the OLS method.

In Table 4, based on the R^2, PBias, RSR, and r metrics, DNN_{PI1} further proved as the best model that exhibited satisfactory performance for all training and testing metrics, for which the

cumulative capacity loss, observed versus simulated capacity loss, and capacity loss data series are presented in Fig. 6. However, notably, the DNN_{PI1} model appears more accurate at estimating lower levels of cumulative capacity loss on the testing data until it reaches records with capacity loss values of greater than 1.23×10^8 m^3.

Consequently, the model recommended for capacity loss prediction is a calibrated DNN_{PI1} model. The calibrated DNN_{PI1} was established through training the original best performing DNN_{PI1} model on the entire RFE dataset. This was conducted to overcome potential inaccuracies associated with the limited records available, which is the case with the current RSI dataset. For this calibrated model, the R^2 increased to 0.81 and the MAPE value decreased to 38%, as shown in Table 3. This shows significant improvement in terms of forecasting accuracy, compared to all models. Figure 4 illustrates the observed versus predicted capacity loss values for the calibrated DNN_{PI1}. Thus, the model successfully learned on the training dataset, producing satisfactory performance metrics. However, high accuracy determinations for larger amounts of capacity loss still appear limited.

5. Conclusions

A composite dataset was developed which included capacity loss data obtained from RSI system records and 29 supplemental parameters derived from publicly available databases. The composite dataset included 184 reservoirs, 799 surveys, and 615 sets of consecutive surveys for evaluating capacity loss. The study demonstrated that prediction models containing supplemental data inputs estimate reservoir capacity loss (acre-ft) with satisfactory R^2, PBias, RSR, and r values as defined in Moriasi et al., 2007. Of the nine predictive models, the progressively increasing deep neural network (DNN_{PI1}) had the best predictive performance with model training and testing R^2 values

of 0.83 and 0.70, respectively; and training and testing MAPE of 87% and 295%, respectively. Notably, the DNN_{PI1} had higher accuracy at predicting capacity loss values lower than 1.23×10^8 m^3. The DNN_{PI1} model was recalibrated over the entire dataset with resulting R^2 and mean absolute percent error (MAPE) values of 0.81 and 48%, respectively. Accordingly, the DNN_{PI1} is the most promising model for estimating reservoir capacity losses using watershed and historical precipitation data which enables the identification of vulnerable reservoirs within the US. Further, the DNN_{PI1} model can be used to forecast reservoir sedimentation rates under possible future climate scenarios which allows for the development of proactive management plans.

6. Acknowledgements

This research was supported by the U.S. National Science Foundation (Award # 1948940) and the WATER Institute at Saint Louis University.

7. References

Abrahart, R. J., & White, S. M. (2001). Modelling sediment transfer in Malawi: comparing backpropagation neural network solutions against a multiple linear regression benchmark using small datasets. *Physics and Chemistry of the Earth, Part B: Hydrology, Oceans and Atmosphere, 26*(1), 19-24.

Adler, J., & Parmryd, I. (2010). Quantifying colocalization by correlation: the Pearson correlation coefficient is superior to the Mander's overlap coefficient. *Cyotemtry Part A, 77*(8), 733-742.

Adnan, M. S., Dewan, A., Zannat, K. E., & Abdullah, A. M. (2019). The use of watershed geomorphic data in flash flood susceptibility zoning: a case study of the Karnaphuli and Sangu river basins of Bangladesh. *Natural Hazards, 99*, 425-448.

Alexopoulos, E. C. (2010). Introduction to multivariate regression analysis. *Hippokratia, 14*(1), 23-28.

Austin, P. C., & Steyerberg, E. C. (2015). The number of subjects per variable required in linear regression analyses. *Journal of Clinial Epidemiology, 68*(6), 627-636. doi:http://dx.doi.org/10.1016/j.jclinepi.2014.12.014

Ayele, G. T., Teshale, E. Z., Yu, B., Rutherfurd, I. D., & Jeong, J. (2017). Streamflow and sediment yield prediction for watershed prioritization in the Upper Blue Nile River Basin. *Water, 9*(10), 782.

Baniya, B., Tang, Q., Xu, X., Haile, G. G., & Chhipi-Shrestha, G. (2019). Spatial and temporal variation of drought based on satellite derived vegetation condition index in Nepal from 1982-2015. *Sensors, 19*(2), 430.

Bashar, S. S., Miah, M. S., Zadidul Karim, A., & Al Mahmud, M. (2019). Extraction of Heart Rate from PPG signal: A Machine Learning Approach using Decision Tree Regression Algorithm. *4th International Conference on Electrical Information Communication Technology (EICT)*, (pp. 1-6). Khulna, Bangladesh.

Bon-Gang, H. (2018). *Performance and Improvement of Green Construction Projects: Management Strategies and Innovations.* Butterworth-Heinemann.

Brakstad, F. (1992). A Comprehensive Pollution Survey of Polychlorinated Dibenzo-P-Dioxins and Dibenzofurans by Means of Principal Component Analysis and Partial Least-Squares Regression. *Chemosphere, 24*(12), 1885-1903.

Breiman, L. (2001). Random Forests. *Machine Learning, 45*, 5-32. doi:http://dx.doi.org/10.1023/A:1010933404324

Brown, C. B. (1943). Discussion in Sedimentation in Reservoirs. (B. J. Witzig, Ed.) *Transactions of the American Society of Civil Engineers, 109*, 1047-1106.

Cao, X. H., Stojkovic, I., & Obradovic, Z. (2016). A robust data scaling algorithm to improve classification accuracies in biomedical data. *BMC Bioinformatics, 17*(1), 1-10.

Choubin, B. H., Darabi, H., Rahmati, O., Sajedi-Hosseini, F., & Klove, B. (2017). River suspended sediment modelling using the CART Model: A comparative study of machine learning techniques. *Science of The Total Environment*, 615:272-281.

Daly, C., Smith, J. I., & Olson, K. V. (2015). Mapping atmospheric moisture climatologies across the conterminous United States. *PloS One, 10*(10), e0141140.

Demiray, B. Z., Sit, M., & Demir, I. (2021). D-SRGAN: DEM super-resolution with generative adversarial networks. *SN Computer Science, 2*(1), 1-11.

Emmerson, R. H., O'Reilly-Wiese, S., Macleod, C., & Lester, J. (1997). A multivariate assessment of metal distribution in inter-tidal sediments of the Blackwater Estuary, UK. *Marine Pollution Bulletin, 34*(11), 960-968.

Gautam, A., Sit, M., & Demir, I. (2022). Realistic river image synthesis using deep generative adversarial networks. *Frontiers in Water, 4*.

Goodfellow, I., Bengio, Y., & Courville, A. (2016). *Deep Learning*. MIT Press.

Gorelick, N., Hancher, M., Dixon, M., Ilyushchenko, S., Thau, D., & Moore, R. (2017). Google Earth Engine: Planetary-scale geospatial analysis for everyone. *Remote Sensing of Environment, 202*, 18-27.

Goyal, H., Sandeep, D., Vanu, R., Pokuri, R., Kathula, S., & Battula, N. (2014). Normalization of Data in Data Mining. *International Journal of Software and Web Sciences, 14*, 32-33.

494 Harrell, F. E. (2001). *Regression Modeling Strategies: With Application to Linear Models,*
495 *Logistic Regression, and Survival Analysis.* Springer.
496 Hazarika, B. B., Gupta, D., & Berlin, M. (2020). Modeling suspended sediment load in a river
497 using extreme learning machine and twin support vector regression with wavelet
498 conjunction. *Environmental Earth Sciences*, 79:1-15.
499 Hecht, R. M., & Tishby, N. (2005). Extraction of relevant speech features using the information
500 bottleneck method. *Interspeech*.
501 Jothiprakash, V., & Garg, V. (2009). Reservoir sedimentation estimation using artificial neural
502 network. *Journal of Hydrologic Engineering, 14*(9), 1035-1040.
503 Legates, D. R., & McCabe Jr., G. J. (1999). Evaluating the use of "goodness-of-fit" measures in
504 hydrologic and hydroclimatic model validation. *Water Resources Research, 35*(1), 233-
505 241.
506 Lehner, B., Liermann, C. R., Revenga, C., Vorosmarty, C., Fekete, B., Crouzet, P., . . . Wisser,
507 D. (2011). High-resolution mapping of the world's reservoirs and dams for sustainable
508 river-flow managment. *Frontiers in Ecology and the Environment, 9*(9), 494-502.
509 Maimaitijiang, M., Sagan, V., Sidike, P., Hartling, S., Esposito, F., & Fritschi, F. (2020).
510 Soybean yield prediction from UAV using multimodal data fusion and deep learning.
511 *Remote Sensing of Environment, 237*, 111599.
512 Manikanta, C., & Mamatha Jadav, V. (2015). Evaluation of modified PLS regression method to
513 fill the missing values in training dataset. *International Conference on Smart Sensors and*
514 *Systems (IC-SSS)*, (pp. 1-5).
515 Montavon, G., Wojciech, S., & Klaus-Robert, M. (2018). Methods for interpreting and

understanding deep neural networks. *Digital Signal Processing, 73*, 1-15.

Moriasi, D. N., Arnold, J., Van Liew, M., Bingner, R., Harmel, R., & Veith, T. (2007). Model evaluation guidelines for systematic quantification of accuracy in watershed simulations. *Transactions of the ASABE, 50*(3), 885-900.

Morris, G., & Fan, J. (1998). *Reservoir Sedimentation Handbook: Design and Management of Dams, Reservoirs, and Watershed for Sustainable Use.* New York: McGraw-Hill.

Noble, W. S. (2006). *What is a support vector machine?* Retrieved 2021, from Nature.com: https://www.ifi.uzh.ch/dam/jcr:00000000-7f84-9c3b-ffff-ffffc550ec57/what_is_a_support_vector_machine.pdf

Patro, S., & Sahu, K. (2015). Normalization: A Preprocessing Stage. *ArXiv, abs/1503.06462*.

Pinson, A., Baker, B., Boyd, P., Grandpre, R., White, K., & Jonas, M. (2016, 05). U.S. Army Corps of Engineers Reservoir Sedimentation in the Context of Climate Change. *Civil Works Technical Report (CWTS) 2016-05*.

Randle, T., Morris, G., Tullos, D., Weirich, F., Kondolf, G., Moriasi, D., & Wegner, D. (2021). Sustaining United States reservoir storage capacity: Need for a new paradigm. *Journal of Hydrology, 602*, 126686.

Renard, K. G. (1997). *Predicting soil erosion by water: a guide to conservation planning with the Revised Universal Soil Loss Equation (RUSLE).* United States Government Printing.

Sholtes, J., Ubing, C., Ranndle, T., Fripp, J., Cenderelli, D., & Baird, D. (2018). Managing infrastructure in the stream environment. *Journal of the American Water Resources Association, 54*(6), 1172-1184.

Singh, A., Thakur, N., & Sharma, A. (2016). A review of supervised machine learning

algorithms. *3rd International Conference on Computing for Sustainable Global Development (INDIACom)* (pp. 1310-1315). IEEE.

Taylor, R. (1990). Interpretation of the Correlation-Coefficient - a Basic Review. *Journal of Diagnostic Medical Sonography, 6*(1), 35-39. doi:10.1177/875647939000600106.

Tishby, N., Pereira, F., & Bialek, W. (2000). The information bottleneck method. *arXiv preprint physics/0004057*.

Trimble, S. W. (1999). Decreased rates of alluvial sediment storage in the Coon Creek Basin, Wisconsin, 1975-93. *Science, 285*(5431), 1244-1246.

US Geological Survey. (2017). 1/3rd arc-second Digital Elevation Models (DEMs) - USGS National Map 3DEP Downloadable Data Collection.

Verstraeten, G., Poesen, J., de Vente, J., & Koninckx, X. (2003). Sediment yield variability in Spain: a quantitative and semiqualitative analysis using reservoir sedimentation rates. *Geomorphology, 50*(4), 327-348.

Viger, R. J., & Bock, A. (2014). GIS features of the geospatial fabric for nation hydrologic modeling. *US Geological Survey*. doi:https://doi. org/10.5066/F7542KMD

Vorosmarty, C., Meybeck, M., Fekete, B., Sharma, K., Green, P., & Syvitski, J. (2003). Anthropogenic sediment retention: Major global impact from registered river impoundments. *Global and Planetary Change, 39*, 169-190.

Xiang, Z., & Demir, I. (2020). Distributed long-term hourly streamflow prediction using deep learning - A case study for State of Iowa. *Environmental Modelling & Software, 131*, 104761.

Xu, H., Demir, I., Koylu, C., & Muste, M. (2019). A web-based geovisual analytics platform

foridentifying potential contributors to culvert sedimentation. *Science of the Total Environment, 692*, 806-817.

Zdaniuk, B. (2014). Ordinary Least Squares (OLS) Model. *Encyclopedia of Quality of Life and Well-Being Research*. doi:http://dx.doi.org/10.1007/978-94-007-0753-5_2008

Zounemat-Kermani, M., Kisi, O., Piri, J., & Mahdavi-Meymand, A. (2019). Assessment of artificial intelligence-based models and metaheuristic algorithms in modeling evaporation. *Journal of Hydrologic Engineering, 24*(10), 04019033.

Zounemat-Kermani, M., Mahdavi-Meymand, A., Alizamir, M., Adarsh, S., & Yaseen, Z. (2020). On the complexities of sediment load modeling using integrative machine learning: Application of the great river of Loiza in Puerto Rico. *Journal of Hydrology, 585*, 124759.

572 **Table 1.** Recursive Feature Eliminated (RFE) ranked dataset variables

Index	Variable	Units Imperial (SI)	Metric Unit Conversion Factor	Calibrated Standard Scaled Data - OLS Coefficients	Calibrated Unscaled Data - OLS Coefficients
1	Basin Area	mi^2 (km^2)	0.386	1.42	0.553
2	Initial Capacity	acre-ft (m^3)	8.11×10^{-4}	1.03	0.476
3	Cumulative Precipitation	in (mm)	3.93×10^{-2}	0.323	0.383
4	Hydraulic Length	ft (m)	3.28	-0.259	-0.181
5	Max Monthly Precipitation	in (mm)	3.93×10^{-2}	0.234	0.561
6	Curve Number	n/a	-	0.144	1.63
7	Total Upstream Dam Height	ft (m)	3.28	-0.119	-0.0494
8	Total Upstream Normal Storage	acre-ft (m^3)	8.11×10^{-4}	0.100	0.0250
9	Basin Relief	ft (m)	3.28	-0.0369	-0.0267
10	Channel Slope	ft/ft (m/m)	1.00	0.0226	1.91
11	Average Basin Latitude	°	-	0.0197	0.192
12	Mean Monthly Precipitation	in/mo. (mm/mo.)	3.93×10^{-2}	0.0158	0.0589

573

574 **Table 2.** Summary statistics for capacity loss models based on untransformed data

MODEL	Untransformed Statistics											
	Training						Testing					
	R^2	MAE	MAPE	RRMSE	RMSE	MSE	R^2	MAE	MAPE	RRMSE	RMSE	MSE
OLS	0.54	1.3E+07	220	155	3.6E+07	1.1E+12	0.36	3.2E+07	74	298	1.5E+08	1.9E+13
SVM	0.24	2.5E+07	165	323	1.2E+08	1.1E+13	0.38	1.7E+07	109	194	5.1E+07	2.1E+12
RFR	0.61	1.4E+07	40	232	8.2E+07	5.5E+12	0.57	1.4E+07	254	162	4.2E+07	1.5E+12
DTR	1.00	0	0	0	0	0	0.12	2.2E+07	1268	231	6.0E+07	3.0E+12
PLS	0.38	2.1E+07	211	294	1.0E+08	8.9E+12	0.53	1.4E+07	145	169	4.4E+07	1.6E+12
DNN_{PI1}	0.83	1.4E+07	87	155	5.5E+07	2.5E+12	0.70	1.3E+07	295	135	3.5E+07	1.0E+12
DNN_{PD1}	0.72	2.3E+07	106	198	7.0E+07	4.0E+12	0.45	2.0E+07	327	182	4.8E+07	1.8E+12
DNN_{PI2}	0.17	2.5E+07	187	339	1.2E+08	1.2E+13	0.35	1.7E+07	282	199	5.2E+07	2.2E+12
DNN_{PD2}	0.41	2.1E+07	189	287	1.0E+08	8.4E+12	0.39	1.6E+07	333	192	5.0E+07	2.0E+12
*Calib. OLS	0.40	1.9E+07	195	280	8.9E+07	6.4E+12	-	-	-	-	-	-

575

576 **Table 3.** Untransformed metrics. Highlighted cells indicate satisfactory metrics

MODEL	Untransformed Statistics							
	Training				Testing			
	R^2	PBIAS(%)	RSR	r	R^2	PBIAS(%)	RSR	r
OLS	0.54	29.45	0.67	0.75	0.36	57.79	0.80	0.80
SVM	0.24	59.57	0.87	0.68	0.38	54.20	0.79	0.78
RFR	0.61	34.35	0.62	0.92	0.57	40.47	0.66	0.85
DTR	1.00	0	0	1.00	0.12	9.15	0.94	0.50
PLS	0.38	41.87	0.79	0.71	0.53	35.87	0.69	0.79
DNN_{PI1}	0.83	14.77	0.42	0.94	0.70	12.49	0.55	0.84
DNN_{PD1}	0.72	-32.77	0.53	0.88	0.45	-37.95	0.74	0.85
DNN_{PI2}	0.17	64.41	0.91	0.64	0.35	56.84	0.81	0.82
DNN_{PD2}	0.41	52.15	0.77	0.84	0.39	46.36	0.78	0.76
*Calib. OLS	0.40	39.03	0.78	0.71	-	-	-	-

577

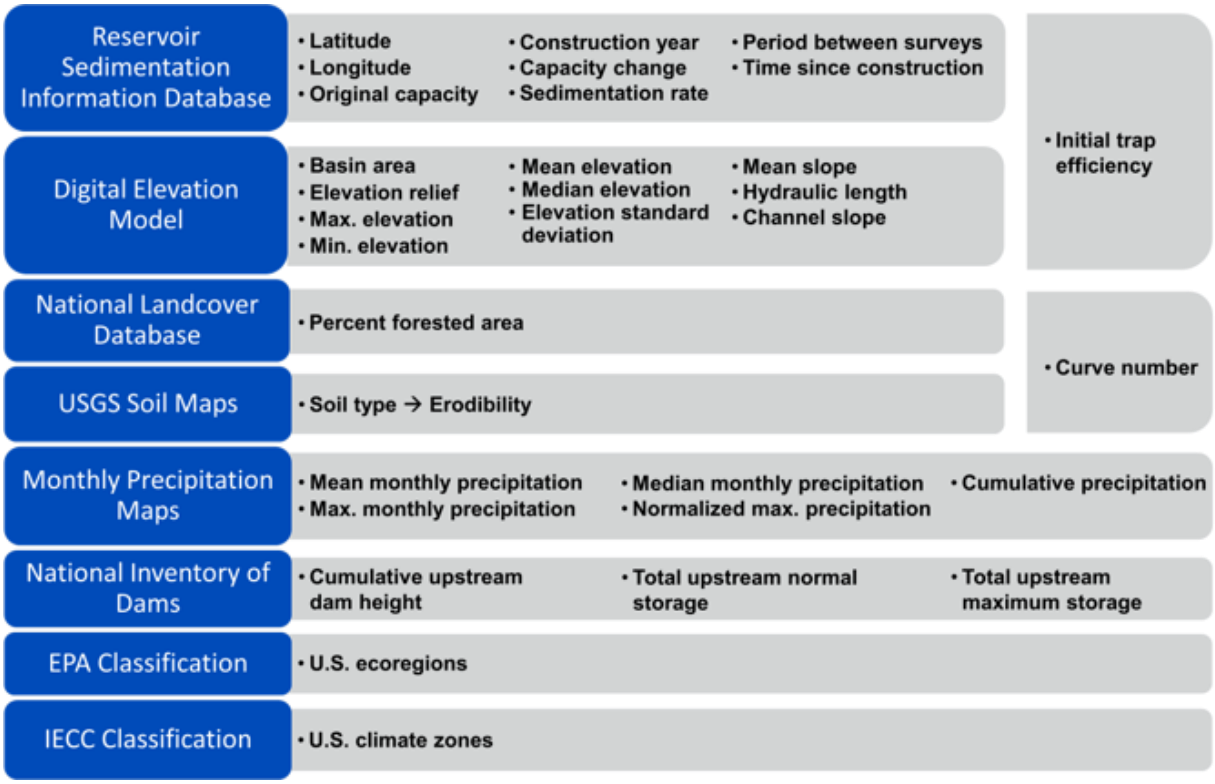

578

579 **Fig. 1**. Data sources and derived variables (numerical and categorical) of the composite RSI
580 dataset. Variables in bold are time dependent

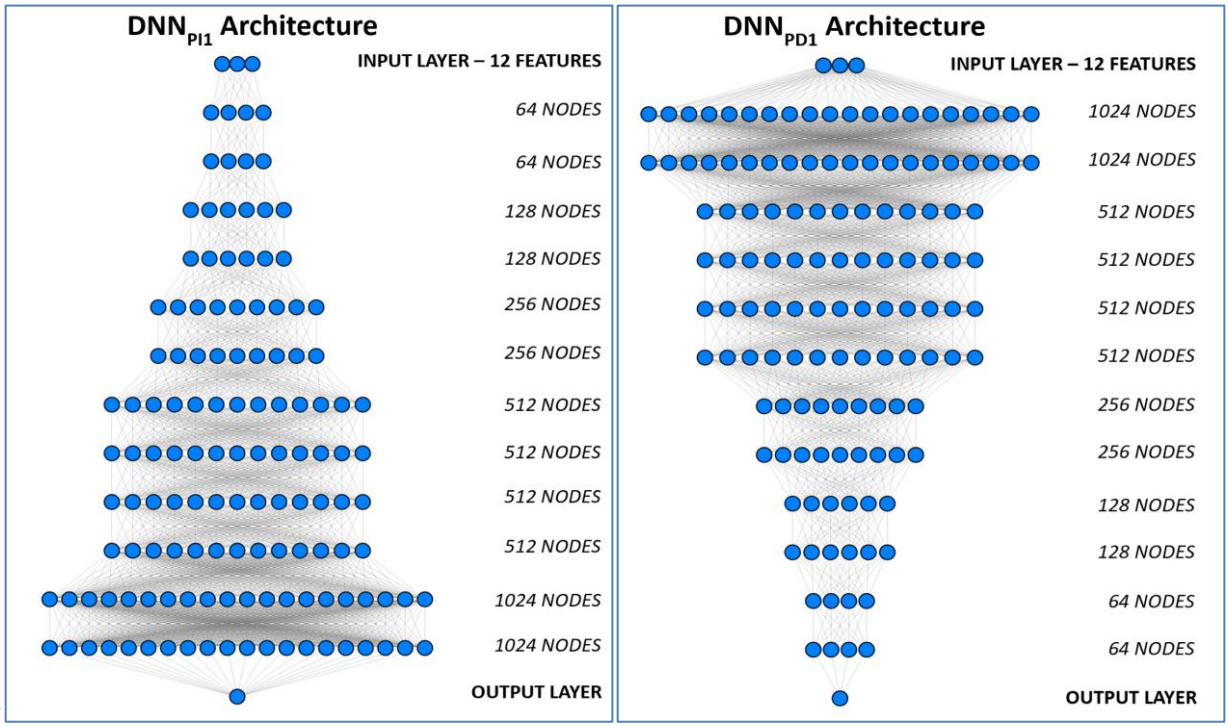

Fig. 2. Diagrams of the hidden-layer architectures of DNNPI1 (left) and DNNPD1 (right) with the respective nodes present in each of their layers

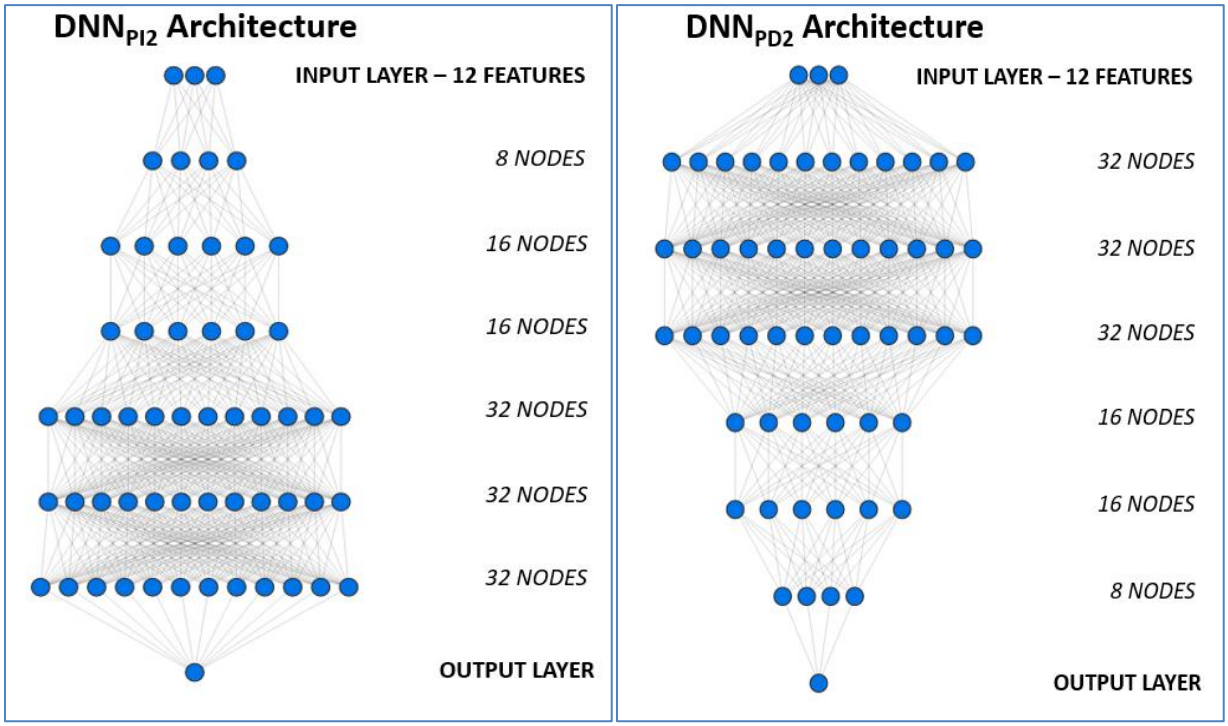

Fig. 3. Diagrams of the hidden layer architectures of DNNPI2 (left) and DNNPD2 (right) with the respective nodes present in each of their layers

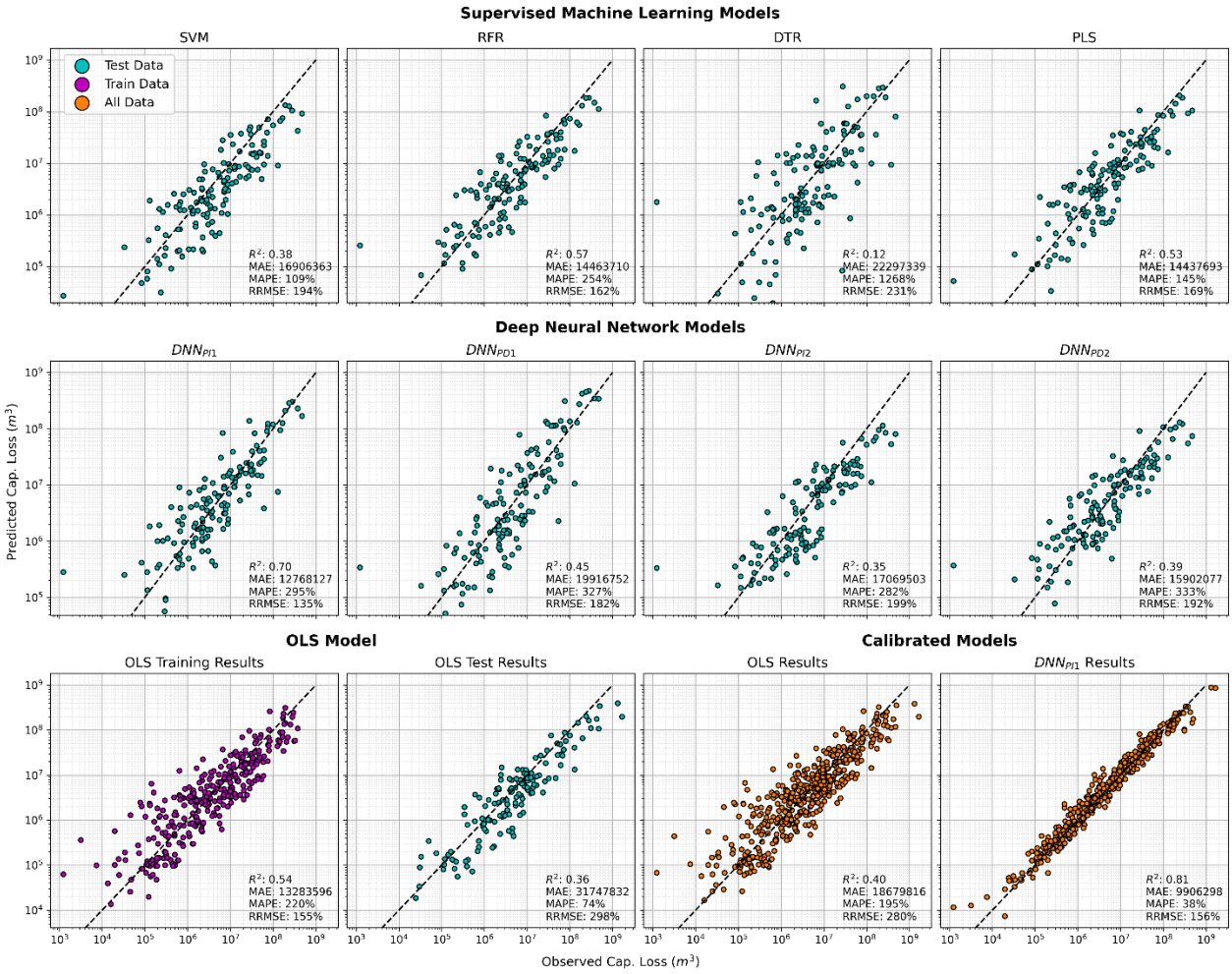

Fig. 4. Comparison of all predictive models

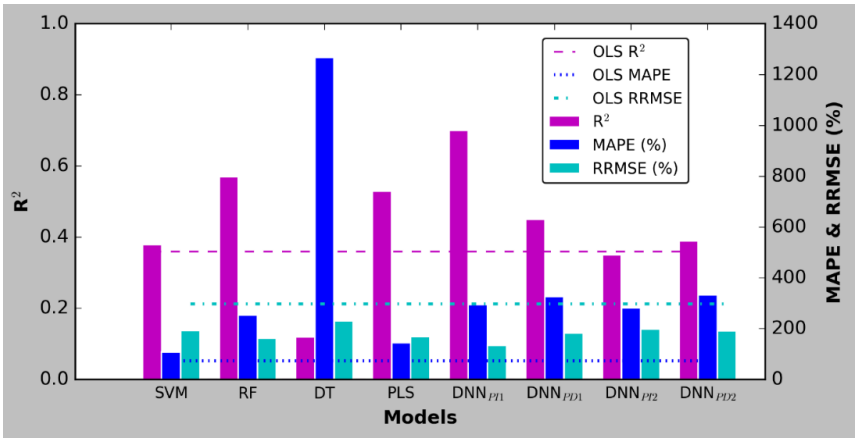

Fig. 5. Comparison of R2, MAPE, and RRMSE values across all models, related to the respective OLS method values

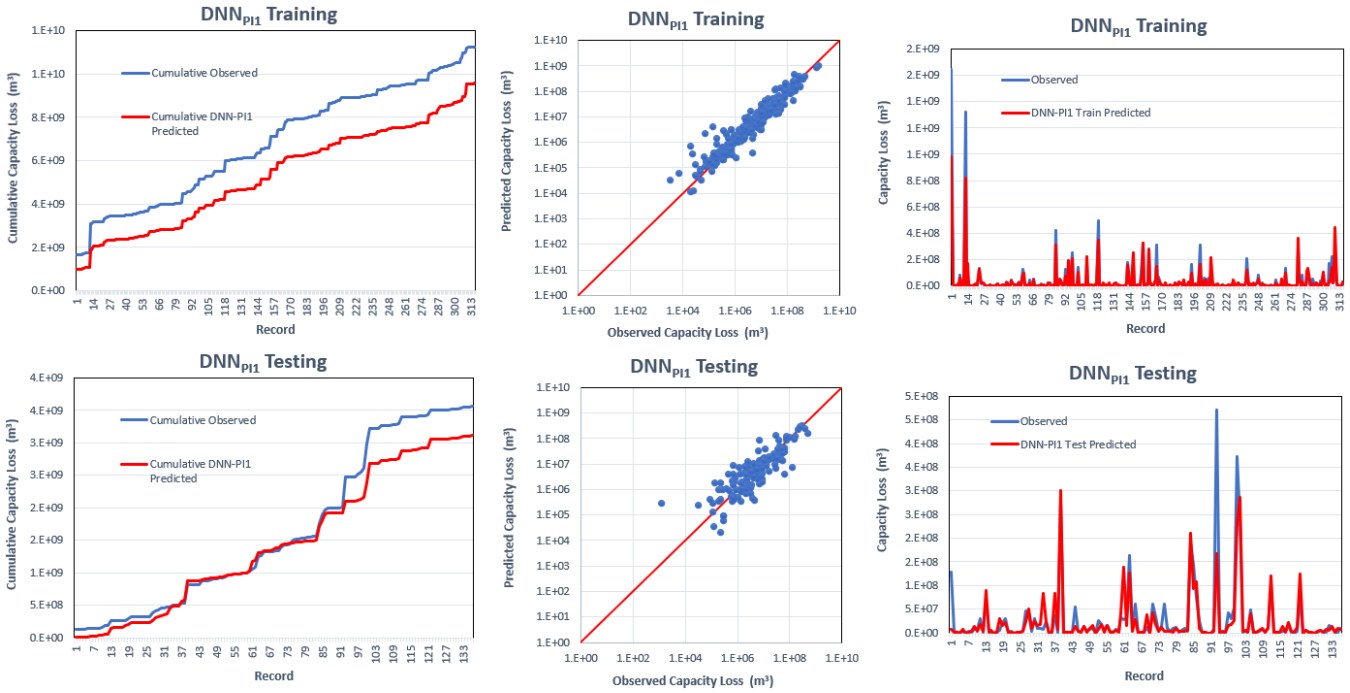

Fig. 6. Cumulative capacity loss, observed vs. simulated capacity loss, and capacity loss data series corresponding to the untransformed metrics for the DNNPI1 machine learning model

List of Table and Figure Captions